

## Origin of two-dimensional electron gas in $\text{Zn}_{1-x}\text{Mg}_x\text{O}/\text{ZnO}$ heterostructures

Xiang-Hong Chen <sup>1</sup>, Dong-Yu Hou,<sup>1</sup> Zhi-Xin Hu <sup>2</sup>, Kuang-Hong Gao,<sup>1,\*</sup> and Zhi-Qing Li <sup>1,†</sup>  
<sup>1</sup>Tianjin Key Laboratory of Low Dimensional Materials Physics and Preparing Technology, Department of Physics,  
 Tianjin University, Tianjin 300354, China

<sup>2</sup>Center for Joint Quantum Studies and Department of Physics, Tianjin University, Tianjin 300354, China



(Received 3 January 2023; revised 21 March 2023; accepted 3 April 2023; published 17 April 2023)

Although the two-dimensional electron gas (2DEG) in (001)  $\text{Zn}_{1-x}\text{Mg}_x\text{O}/\text{ZnO}$  heterostructures was discovered about 20 years ago, the origin of the 2DEG is still inconclusive. In the present paper, the formation mechanisms of 2DEG near the interfaces of (001)  $\text{Zn}_{1-x}\text{Mg}_x\text{O}/\text{ZnO}$  heterostructures were investigated via the first-principles calculations method. It is found that the polarity discontinuity near the interface can neither lead to the formation of 2DEG in devices with thick  $\text{Zn}_{1-x}\text{Mg}_x\text{O}$  layers nor in devices with thin  $\text{Zn}_{1-x}\text{Mg}_x\text{O}$  layers. For a heterostructure with a thick  $\text{Zn}_{1-x}\text{Mg}_x\text{O}$  layer, the oxygen vacancies near the interface introduce a defect band in the band gap, and the top of the defect band overlaps with the bottom of the conduction band, leading to the formation of the 2DEG near the interface of the device. For a heterostructure with a thin  $\text{Zn}_{1-x}\text{Mg}_x\text{O}$  layer, the adsorption of hydrogen atoms, oxygen atoms, or OH groups on the surface of the  $\text{Zn}_{1-x}\text{Mg}_x\text{O}$  film plays a key role for the formation of 2DEG in the device. Our results manifest the sources of 2DEGs in  $\text{Zn}_{1-x}\text{Mg}_x\text{O}/\text{ZnO}$  heterostructures on the electronic structure level.

DOI: [10.1103/PhysRevB.107.165411](https://doi.org/10.1103/PhysRevB.107.165411)

### I. INTRODUCTION

Since the discovery of two-dimensional electron gas (2DEG) at the interface of the  $\text{LaAlO}_3/\text{SrTiO}_3$  heterojunction [1], 2DEG has been found in various oxide heterostructures, such as  $\text{Zn}_{1-x}\text{Mg}_x\text{O}/\text{ZnO}$  [2–4],  $\text{Al}_2\text{O}_3/\text{SrTiO}_3$  [5,6],  $\text{EuO}/\text{KTaO}_3$  [7],  $(\text{Al}_x\text{Ga}_{1-x})_2\text{O}_3/\text{Ga}_2\text{O}_3$  [8], and  $\text{LaAlO}_3/\text{KTaO}_3$  [9]. The 2DEG at oxide heterostructures not only provides a platform for fundamental research, but also promotes the development of novel all-oxide electronic devices. Among these oxide heterostructures,  $\text{Zn}_{1-x}\text{Mg}_x\text{O}/\text{ZnO}$  heterostructures are particularly attractive due to their ultrahigh Hall mobility (up to  $10^6 \text{ cm}^2 \text{ V}^{-1} \text{ s}^{-1}$  at low temperature [10]). However, the origin of the 2DEG at the  $\text{Zn}_{1-x}\text{Mg}_x\text{O}/\text{ZnO}$  interface is still unclear. Researchers only empirically attribute it to the polar discontinuity [11–14]: since  $\text{Zn}_{1-x}\text{Mg}_x\text{O}$  ( $0 < x < 0.6$ ) and  $\text{ZnO}$  have different spontaneous polarizations, the polarization at the interface is discontinuous after they form heterojunctions; this discontinuity causes a large number of bound charges to be generated at the heterointerface, creating a built-in electric field throughout the heterostructure; this field drives electrons toward the interface to form a 2DEG. In contrast, some researchers believe that the 2DEG at the  $\text{Zn}_{1-x}\text{Mg}_x\text{O}/\text{ZnO}$  interface originates from the donor on the  $\text{Zn}_{1-x}\text{Mg}_x\text{O}$  surface [15,16]. Experimentally, 2DEG can also be formed when the thickness of the  $\text{Zn}_{1-x}\text{Mg}_x\text{O}$  layer is greater than 300 nm in  $\text{Zn}_{1-x}\text{Mg}_x\text{O}/\text{ZnO}$  heterostructures [17–20]. There would be no internal potential gradient in the aforementioned heterostructure with a thick

$\text{Zn}_{1-x}\text{Mg}_x\text{O}$  layer, and the contribution of surface donors to 2DEG could also be negligible [21,22]. Thus the formation of 2DEG in this case cannot be explained by the mechanisms mentioned above. On the whole, the origin of 2DEG at the  $\text{Zn}_{1-x}\text{Mg}_x\text{O}/\text{ZnO}$  heterointerface needs to be further studied. In the present paper, the origin of 2DEG at the  $\text{Zn}_{1-x}\text{Mg}_x\text{O}/\text{ZnO}$  heterointerface is studied from the perspective of microscopic electronic structures by first-principles calculations. Interestingly, it is found that the polar discontinuity mechanism is not responsible for the formation of the 2DEG. For heterostructures with thick  $\text{Zn}_{1-x}\text{Mg}_x\text{O}$  layers, 2DEG mainly arises from oxygen vacancies, while the 2DEG originates from surface adsorption for heterostructures with thin  $\text{Zn}_{1-x}\text{Mg}_x\text{O}$  layers.

### II. HETEROSTRUCTURE CONSTRUCTION AND CALCULATION METHOD

We choose the slab model with a  $2 \times 2$   $\text{Zn}_{1-x}\text{Mg}_x\text{O}/\text{ZnO}$  supercell in the (001) plane to simulate the  $\text{Zn}_{1-x}\text{Mg}_x\text{O}/\text{ZnO}$  heterostructure grown along the  $c$  axis. The slab model is often employed in calculating the electronic structures of thin films or two-dimensional materials via the density functional theory (DFT) method. For a slab with two oppositely charged surfaces, there is a constant electric field throughout the slab. In this situation, the electronic structure of the slab is still different from that of the bulk material even if the thickness of the slab is thick enough. To overcome this problem, a modified passivation method proposed by Yoo *et al.* [21] was employed in our calculations. Considering that the 2DEG can be formed in  $\text{Zn}_{1-x}\text{Mg}_x\text{O}/\text{ZnO}$  heterostructures with both thick ( $\sim 100$ – $500$  nm) [23–27] and thin  $\text{Zn}_{1-x}\text{Mg}_x\text{O}$  layers ( $\sim 10$ – $30$  nm) [14–16], experimentally, we construct the

\*Corresponding author: khgao@tju.edu.cn

†Corresponding author: zhiqingli@tju.edu.cn

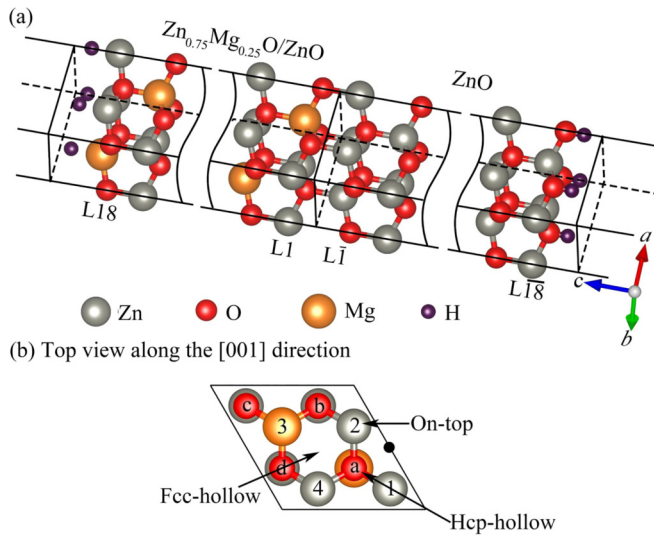


FIG. 1. (a) Schematic geometrical structure of  $\text{Zn}_{0.75}\text{Mg}_{0.25}\text{O}/\text{ZnO}$  heterostructure with two pseudo-H-passivated surfaces. (b) The top view of the heterostructure along the [001] direction. Here, “on-top,” “fcc-hollow,” and “hcp-hollow” are the adsorption sites for exotic atoms or groups.

configurations as follows. For  $\text{Zn}_{1-x}\text{Mg}_x\text{O}/\text{ZnO}$  heterostructures with thick  $\text{Zn}_{1-x}\text{Mg}_x\text{O}$  layers, we passivated the oxygen terminal of the ZnO slab and the Zn-Mg terminal of  $\text{Zn}_{1-x}\text{Mg}_x\text{O}$  slab by pseudo-H atoms with fractional charges. A ZnO slab with a passivated oxygen terminal can be used to simulate the ZnO substrate, and the charge of H is taken as  $0.48e$  with  $e$  being the elementary charge [21]. The charge of the pseudo-H atoms in the passivated Zn-Mg terminal is taken as  $1.52e$  [21]. After passivation, the pseudo-H atoms not only saturate the surface dangling bonds but also make the passivated surface and the adjacent atomic layers exhibit bulk properties [21,28]. In this case, the  $\text{Zn}_{1-x}\text{Mg}_x\text{O}$  and ZnO slabs can be treated as semi-infinite thick films.

Considering the Mg content  $x$  can be as high as 0.60 in  $\text{Zn}_{1-x}\text{Mg}_x\text{O}/\text{ZnO}$  heterostructures experimentally [24], we set the Mg content  $x$  as 0.25 and 0.50, respectively. For each doping level, the Mg ions are uniformly doped into the ZnO film, which, together with the ZnO substrate, forms a heterostructure with a clear interface. For the  $\text{Zn}_{1-x}\text{Mg}_x\text{O}/\text{ZnO}$  heterostructures with thin  $\text{Zn}_{1-x}\text{Mg}_x\text{O}$  layers, the difference in the configuration is that there is no pseudo-H atom at the Zn-Mg terminal. Generally, the unpassivated  $\text{Zn}_{1-x}\text{Mg}_x\text{O}$  (001) surface is unstable and surface adsorption or reconstruction is inevitable [29–32]. Thus, surface adsorption and defects are considered to simulate  $\text{Zn}_{1-x}\text{Mg}_x\text{O}/\text{ZnO}$  heterostructures with thin  $\text{Zn}_{1-x}\text{Mg}_x\text{O}$  layers [26]. As an example, in Fig. 1(a) we give the structure diagram of a  $\text{Zn}_{0.75}\text{Mg}_{0.25}\text{O}/\text{ZnO}$  heterostructure with two surfaces passivated by pseudo-H atoms. The heterostructure contains a  $2 \times 2$  in-plane (001)  $\text{Zn}_{0.75}\text{Mg}_{0.25}\text{O}/\text{ZnO}$  supercell and 18 Zn-Mg-O layers and 18 Zn-O layers. A 15-Å-thick vacuum layer is added along the [001] direction to prevent any unintentional interactions between the slabs. From the interface to surface, the atomic layers on the ZnO side are labeled as  $\text{L}\bar{1}$ ,  $\text{L}\bar{2}$ , ...,  $\text{L}\bar{17}$ , and  $\text{L}\bar{18}$ , while the atomic layers on

the  $\text{Zn}_{0.75}\text{Mg}_{0.25}\text{O}$  side are labeled as L1, L2, ..., L17, and L18, respectively. The top view of Fig. 1(a) along the [001] direction is shown in Fig. 1(b). Three adsorption sites, referred to as on-top, fcc-hollow, and hcp-hollow, are indicated by the arrows. The positions of zinc atoms in each layer are numbered as 1, 2, 3, and 4, respectively. For the Mg doping level  $x = 0.25$  case, the zinc atoms at position 1 are substituted by magnesium atoms in the odd layers, while the zinc atoms at position 3 are replaced in the even layers. For the  $x = 0.50$  situation, the zinc atoms at positions 2 and 4 are replaced by magnesium atoms in each layer.

All calculations are carried out in framework of the DFT using the Vienna *ab initio* simulation package (VASP). The in-plane lattice constants of  $\text{Zn}_{1-x}\text{Mg}_x\text{O}/\text{ZnO}$  ( $x = 0.25$  and 0.50) heterostructures are fixed to those of ZnO during the calculations. It is known that the main deficiency of the DFT method is the underestimation of the band gaps of semiconductors and insulators. To overcome this weakness, a variety of calculation methods, such as DFT+ $U$  [33,34], Heyd-Scuseria-Ernzerhof (HSE) hybrid functional [35], Becke three-parameter Lee-Yang-Parr (B3LYP) hybrid functional [36], meta-generalized gradient approximations (meta-GGAs) [37], and Hedin’s  $GW$  approximation ( $GW$ ) [38] methods have been proposed. Among them, both the HSE hybrid functional and  $GW$  methods can give relatively accurate band-gap values for many classes of solids, but the computation cost is also dramatically increased. Thus, they cannot be applied to very large systems. In practice, the generalized gradient approximation (GGA) parametrized by Perdew-Burk-Ernzerhof plus an on-site Coulomb interaction (GGA+ $U$ ) and the local density approximation plus an on-site Coulomb interaction (LDA+ $U$ ) methods, which can also correct the band gap, were often used in the electronic structure calculations. However, the conventional GGA+ $U$  and LDA+ $U$  calculations [here, conventional GGA+ $U$  (LDA+ $U$ ) method means the Hubbard- $U$  correction is added to the localized electrons orbitals] can only correct the gap partially (not entirely) for a semiconductor with itinerant electrons (such as  $s$  electrons in the outer layer). Recently, Paudel *et al.* [39] calculated the electronic structure of ZnO using a modified LDA+ $U$  method, in which the Hubbard- $U$  corrections were added not only to the Zn- $d$  orbitals but also to the Zn- $s$  orbitals. Their results indicate that the obtained gap (3.3 eV) of ZnO is close to the experimental one (3.37 eV [40]), and the position of the Zn  $d$  bands is also close to the experimental value. The validity of this method in correcting the band gap is also confirmed in  $\text{Ga}_2\text{O}_3$  [41] and  $\text{SnO}_2$  [42].

In this paper, the electronic structure of bulk ZnO is calculated by conventional GGA+ $U$  (the Hubbard- $U$  corrections added in Zn- $3d$  and O- $2p$  orbitals are 8.5 and 7.4 eV, respectively), HSE hybrid functional (HSE06, a mixing parameter of 0.32 is used), and the modified GGA+ $U$  (the Hubbard- $U$  corrections added in Zn- $3d$ , O- $2p$ , and Zn- $4s$  orbitals are 8.5, 7.4, and 29.5 eV, respectively) methods, respectively. It is found that gap values calculated by conventional GGA+ $U$ , HSE, and modified GGA+ $U$  methods are 2.48, 3.34, and 3.34 eV, respectively, i.e., the gap value obtained by the modified GGA+ $U$  method is consistent with that by the HSE method and close to the experimental value. However, the conduction band calculated by the modified GGA+ $U$  is

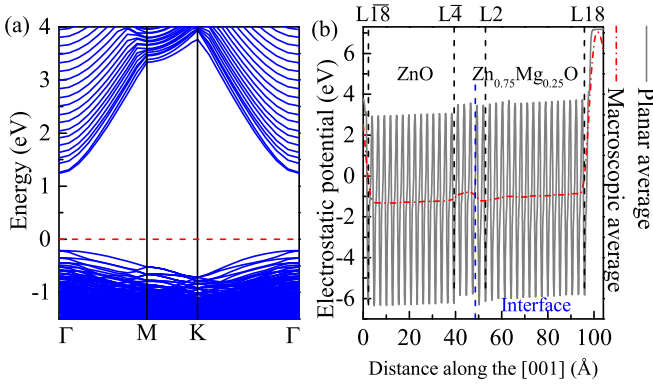


FIG. 2. (a) The energy band structure of the  $\text{Zn}_{0.75}\text{Mg}_{0.25}\text{O}/\text{ZnO}$  heterostructure without oxygen vacancies and with two pseudo-H-atom-passivated surfaces. (b) The plane average (solid curve) and macroscopic average (dashed-dotted curve) electrostatic potential (seen by electron) across the  $\text{Zn}_{0.75}\text{Mg}_{0.25}\text{O}/\text{ZnO}$  heterostructure along the  $[001]$  direction.

compressed (the energy-momentum dispersion curves are more flat compared with those obtained by the other two methods), while the shape of the conduction band calculated by the conventional  $\text{GGA}+U$  method is almost identical to that by the HSE approach. In our configurations, the  $\text{Zn}_{1-x}\text{Mg}_x\text{O}/\text{ZnO}$  ( $x = 0.25$  and  $0.50$ ) heterostructures contain too many atoms (ranging from 295 to 486), which results in the calculations being too expensive to be carried out via the HSE method. Thus, to ensure the shape and curvature of the energy-momentum dispersion curves in the conduction band are not changed, the presented results in this paper are calculated via the conventional  $\text{GGA}+U$  method if there are no special remarks. The modified  $\text{GGA}+U$  calculation is only used to determine whether the heterostructure exhibits semiconductor or metal characteristics in the band structure. For the conventional  $\text{GGA}+U$  method, the Hubbard interaction parameter  $U$  is taken as 8.5 eV (7.4 eV) for the  $\text{Zn-}3d$  ( $\text{O-}2p$ ) orbital, while for the modified  $\text{GGA}+U$  method, the Hubbard interaction parameters added in the  $\text{Zn-}3d$  and  $\text{O-}2p$  orbitals are retained, and the  $U$  added in  $\text{Zn-}4s$  orbitals is 29.5 eV. The plane-wave cutoff energy was set as 500 eV and a Brillouin zone with  $4 \times 4 \times 1$  Monkhorst-Pack  $\mathbf{k}$ -point grids was employed. The structure relaxation was finished until the residual force was smaller than  $0.03 \text{ eV}/\text{\AA}$ . To remove the undesired electrostatic interaction between periodic cells along the  $z$  direction, the dipole correction is applied.

### III. RESULTS AND DISCUSSIONS

Figure 2(a) shows the band structure of  $\text{Zn}_{0.75}\text{Mg}_{0.25}\text{O}/\text{ZnO}$  heterostructure shown in Fig. 1(a) (i.e., the heterostructure has 18 Zn-O and 18 Zn-Mg-O layers and two pseudo-H-atom-passivated surfaces). Clearly, the valence band maximum and the conduction band minimum are both located at the  $\Gamma$  point, and the Fermi level lies in the band gap. Thus the energy band of the  $\text{Zn}_{0.75}\text{Mg}_{0.25}\text{O}/\text{ZnO}$  heterostructure exhibits direct-gap semiconductor characteristics (the calculated band gap is 1.45 eV) and no 2DEG is formed at the interface. For the  $x = 0.50$  case, the band structure is

similar to that of the  $x = 0.25$  and the calculated band gap is 1.56 eV. Therefore, 2DEG cannot appear near the interfaces of the perfect  $\text{Zn}_{1-x}\text{Mg}_x\text{O}/\text{ZnO}$  ( $x = 0.25$  and  $0.50$ ) heterostructures (without defects) with thick  $\text{Zn}_{1-x}\text{Mg}_x\text{O}$  layers. We also calculated the electrostatic potential distribution for the above heterostructures, and Fig. 2(b) presents the results for the  $x = 0.25$  case as an example. There is a conspicuous bulge in the macroscopic average potential curve near the interface (from the  $L\bar{4}$  Zn-O layer to the  $L2$  Zn-Mg-O layer). In the atomic layers away from the interface, e.g., the Zn-O layers from  $L\bar{4}$  to  $L18$  or Zn-Mg-O layers from  $L2$  to  $L18$ , the average potential almost retains a constant. Thus, a potential barrier rather than a quantum well is formed near the interface of the  $\text{Zn}_{0.75}\text{Mg}_{0.25}\text{O}/\text{ZnO}$  heterostructure. Similar phenomena are also observed in the macroscopic average potential curve of the  $\text{Zn}_{0.5}\text{Mg}_{0.5}\text{O}/\text{ZnO}$  heterostructure. This potential barrier should be caused by the polar discontinuity at the interface, which could induce a localized polarization field near the interface. The polarization field cannot cause the bottom of the conduction band to overlap with the top of the valence band as in the case of  $\text{LaAlO}_3/\text{SrTiO}_3$  heterostructures [43]. Thus, polar discontinuity alone cannot explain the observed 2DEG near the interface of a  $\text{Zn}_{1-x}\text{Mg}_x\text{O}/\text{ZnO}$  heterostructure with a thick  $\text{Zn}_{1-x}\text{Mg}_x\text{O}$  layer.

Then, why can the 2DEGs be formed in  $\text{Zn}_{1-x}\text{Mg}_x\text{O}/\text{ZnO}$  heterostructures with thick  $\text{Zn}_{1-x}\text{Mg}_x\text{O}$  layers? It should be noticed that as intrinsic defects in ZnO and  $\text{Zn}_{1-x}\text{Mg}_x\text{O}$  films, oxygen vacancies are inevitable during device fabrication and could play crucial roles for the formation of 2DEG in  $\text{Zn}_{1-x}\text{Mg}_x\text{O}/\text{ZnO}$  heterostructures [35,44–46]. Next, we investigate the effect of oxygen vacancies on the electronic structures of  $\text{Zn}_{1-x}\text{Mg}_x\text{O}/\text{ZnO}$  ( $x = 0.25$  and  $0.50$ ) heterostructures with thick  $\text{Zn}_{1-x}\text{Mg}_x\text{O}$  layers. First, we calculate the formation energy of oxygen vacancies ( $E_f$ ) in each atomic layer of the above heterostructures. In the oxygen-rich limit,  $E_f$  can be written as [47]

$$E_f = E(V_O) - (E_0 - 0.5E_{O_2}), \quad (1)$$

where  $E(V_O)$  and  $E_0$  are the calculated total energies of the  $\text{Zn}_{1-x}\text{Mg}_x\text{O}/\text{ZnO}$  ( $x = 0.25$  and  $0.50$ ) heterostructures with and without oxygen vacancies, and  $E_{O_2}$  is the calculated total energy of the single  $\text{O}_2$  molecule. For the configuration in Fig. 1, each in-plane supercell contains four oxygen atoms, whose positions are labeled as a, b, c, and d, respectively. The oxygen atoms at d positions are removed in a certain fixed layer to create oxygen vacancies in the calculations. Figure 3 shows the formation energies of the oxygen vacancies in each layer of the  $\text{Zn}_{0.75}\text{Mg}_{0.25}\text{O}/\text{ZnO}$  and  $\text{Zn}_{0.5}\text{Mg}_{0.5}\text{O}/\text{ZnO}$  heterostructures with 18 Zn-O and 18 Zn-Mg-O layers, and two pseudo-H-passivated surfaces. Inspection of Fig. 3 indicates that the overall variation trends of the  $E_f$  versus layer number curves for the two heterostructures are similar. Thus we only discuss the variation of  $E_f$  in the  $\text{Zn}_{0.75}\text{Mg}_{0.25}\text{O}/\text{ZnO}$  heterostructure. On the ZnO side, the value  $E_f$  keeps as a constant in the first two layers, and then sharply increases with increasing layer number, reaches its maximum at  $L\bar{4}$ , then decreases with further increasing layer number, and tends to be saturated as the layer number is greater than 9. On the  $\text{Zn}_{0.75}\text{Mg}_{0.25}\text{O}$  side, the values of  $E_f$  near the interface ( $L1$ – $L6$  Zn-Mg-O layers) vary between  $-0.3$  and  $-0.1$  eV, while those

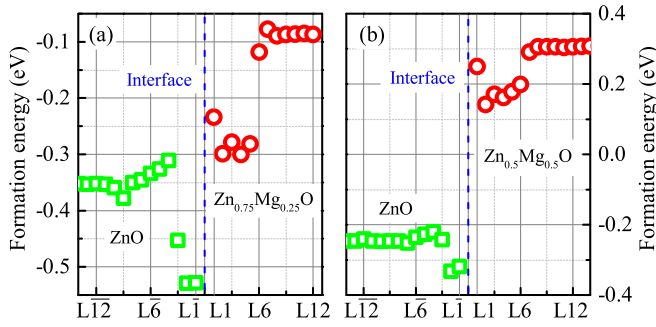


FIG. 3. Formation energies of oxygen vacancies at different atomic layers in  $Zn_{1-x}Mg_xO/ZnO$  heterostructures with two pseudo-H-passivated surfaces. (a) For the  $x = 0.25$ , and (b) for the  $x = 0.50$  heterostructures.

for the layers with the layer number being greater than 6 are almost fixed at  $-0.1$  eV. Obviously, the oxygen vacancies can be easily formed on the ZnO side, especially in the first two Zn-O layers near the interface.

Considering the variation trends in electronic structures with  $V_O$  position for the  $x = 0.25$  and  $0.50$  heterostructures with two pseudo-H passivated surfaces are also similar, we only present and discuss the results obtained from the  $x = 0.25$  ones. We first discuss the case that oxygen vacancies are located at the most easily formed position (L1 layer). Figure 4(a) presents the band structure of this configuration. From this figure, one can see that the oxygen vacancies in the L1 Zn-O layer introduce a defect band in the band gap and the top of the defect band is higher than the Fermi level. At the same time, the Fermi level enters into the bottom of the conduction band, i.e., the conduction band overlaps with the defect band. Thus, part of the electrons in the defect band

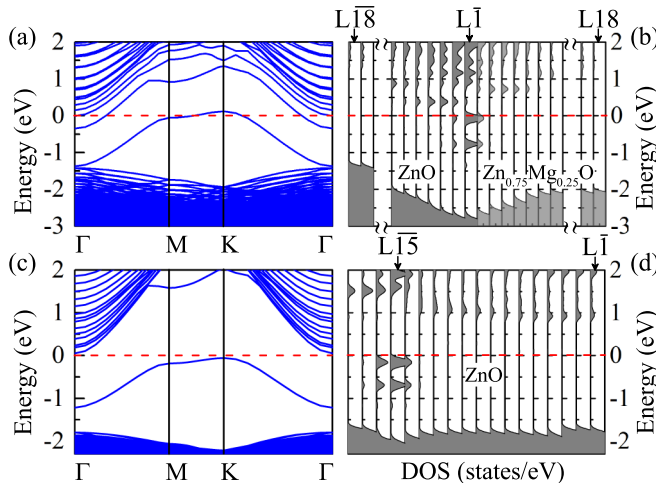


FIG. 4. (a) The band structure of a  $Zn_{0.75}Mg_{0.25}O/ZnO$  heterostructure with oxygen vacancies in the L1 Zn-O layer. (b) The partial DOS projected onto atomic planes for the  $Zn_{0.75}Mg_{0.25}O/ZnO$  heterostructure with oxygen vacancies in the L1 Zn-O layer. (c) The band structure of a  $Zn_{0.75}Mg_{0.25}O/ZnO$  heterostructure with oxygen vacancies in the L15 Zn-O layer. (d) The partial DOS projected onto atomic planes for the  $Zn_{0.75}Mg_{0.25}O/ZnO$  heterostructure with oxygen vacancies in the L15 Zn-O layer.

would be transferred into the conduction band and become conduction electrons. Figure 4(b) shows the partial density of states (DOS) projected onto atomic planes for an  $x = 0.25$  heterostructure with oxygen vacancies in the L1 Zn-O layer and two pseudo-H-passivated surfaces. Clearly, only in L2, L1, and L1 layers the DOS near the Fermi level is nonzero, i.e., the conduction electrons are concentrated in the two Zn-O layers and one Zn-Mg-O layer near the interface. These three layers occupy a space with thickness  $\sim 8.4$  Å, which indicates that the 2DEG is formed near the interface of the heterostructure. From the orbital DOS of L2 to L1 layers, it is found that these conduction electrons are mainly composed of Zn-4s and O-2p orbitals (not shown). In addition, it is found that when the oxygen vacancies are located in the L2 and L3 Zn-O layers and the L1 to L6 Zn-Mg-O layers, their band structures are similar to that in Fig. 4(a). However, the band structures of the heterostructures would reveal semiconductor characteristics when the oxygen vacancies are far from the interface (i.e., behind the L3 Zn-O layer and L6 Zn-Mg-O layer).

We take the  $Zn_{0.75}Mg_{0.25}O/ZnO$  heterostructure with oxygen vacancies in the L15 Zn-O layer as an example. Figure 4(c) shows the band structure of this configuration. The oxygen vacancies in the L15 Zn-O layer also introduce a defect band in the gap, while the top of the defect band is located at 0.11 eV below the bottom of the conduction band. The Fermi level lies between the conduction band and the defect band. Therefore, the introduction of oxygen vacancies in the L15 Zn-O layer cannot induce 2DEG at the interface of the heterostructure. Figure 4(d) shows the partial DOS projected onto atomic planes for the  $Zn_{0.75}Mg_{0.25}O/ZnO$  heterostructure with oxygen vacancies in the L15 Zn-O layer. From this figure, one can see that the defect band of the oxygen vacancies is in fact composed of a large number of deep energy levels as far as the energy band of the inner atomic layer is concerned. These deep levels cannot overlap with the conduction band even if the bottom conduction band of the Zn-O layer near the interface is lower than that of the inner Zn-O layer. On the contrary, the defect levels of the oxygen vacancies near the interface layers are so shallow that the bottom of the conduction band overlaps with the top of the defect band [see Fig. 4(b)]. This is why 2DEG exists only when the oxygen vacancies are located near the interface of the heterostructure. On the other hand, the defect band formed by oxygen vacancies of inner Zn-O layers could enhance the conductivity of the heterostructure. The device will exhibit a thermal-activated form of conductance with activation energy  $E_a$ , where  $E_a$  is about half of the energy difference between the bottom of conduction band and the top of the defect band. Summarizing the results mentioned above, one can readily conclude that the oxygen vacancies near the interface are the origin of the 2DEGs in  $Zn_{1-x}Mg_xO/ZnO$  ( $x = 0.25$  and  $0.50$ ) heterostructures with thick  $Zn_{1-x}Mg_xO$  layers.

Now, we study the origin of 2DEGs in  $Zn_{1-x}Mg_xO/ZnO$  ( $x = 0.25$  and  $0.50$ ) heterostructures when the  $Zn_{1-x}Mg_xO$  films are very thin. In this situation, the influence of the  $Zn_{1-x}Mg_xO$  surface on the electronic structure of the heterostructure near the interface cannot be neglected. The surface on the  $Zn_{1-x}Mg_xO$  side is therefore not passivated,

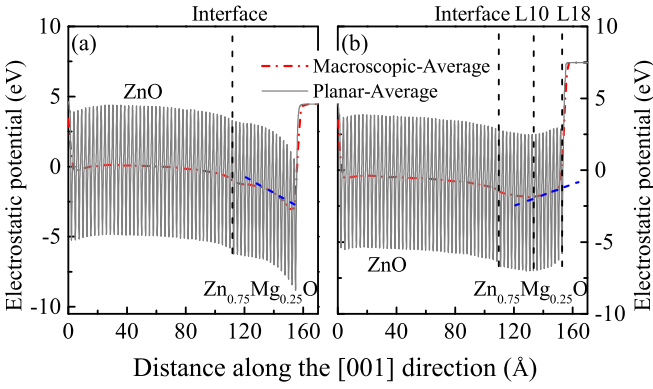


FIG. 5. (a) The plane average (solid curve) and macroscopic average (dashed-dotted curve) electrostatic potential (seen by electron) along the [001] direction for the  $\text{Zn}_{0.75}\text{Mg}_{0.25}\text{O}/\text{ZnO}$  heterostructure, in which only the surface of ZnO film is passivated by pseudo-H atoms. (b) The plane average (solid curve) and macroscopic average (dashed-dotted curve) electrostatic potential (seen by electron) along the [001] direction of the  $\text{Zn}_{0.75}\text{Mg}_{0.25}\text{O}/\text{ZnO}$  heterostructure with a  $\text{Zn}_{0.75}\text{Mg}_{0.25}\text{O}$  surface of hydrogen-atom adsorption.

as mentioned in Sec. II. Initially, we calculated the electronic structures of the heterostructures with 18 Zn-O and 18 Zn-Mg-O layers, in which the surface of the  $\text{Zn}_{1-x}\text{Mg}_x\text{O}$  film was no longer passivated. It is found that the 2DEG can even exist in the L18 layer on the ZnO side (see below for further discussion). Thus the electronic structures of the heterostructures with 42 Zn-O and 18 Zn-Mg-O layers (the surface of the  $\text{Zn}_{1-x}\text{Mg}_x\text{O}$  film is not passivated) are calculated and discussed below. Since the results obtained from the  $x = 0.25$  and  $0.50$  heterostructures are also similar, we only present and discuss the results for the  $x = 0.25$  heterostructure. Figure 5(a) shows the electrostatic potential of the  $\text{Zn}_{0.75}\text{Mg}_{0.25}\text{O}/\text{ZnO}$  heterostructure (with 42 Zn-O and 18 Zn-Mg-O layers) in which only the surface of the ZnO film is passivated by pseudo-H atoms. Obviously, the macroscopic average potential on the ZnO side is insensitive to the position, while it decreases with increasing distance to the interface on the  $\text{Zn}_{0.75}\text{Mg}_{0.25}\text{O}$  side. A macroscopic field perpendicular to the surface with a magnitude of  $0.06 \text{ V}/\text{\AA}$  is obtained by linear fitting the macroscopic average electrostatic potential. This kind of field or potential would lead to an instability of the (001) polar (so-called Tasker type III) surface [30,48]. In light of recent experimental and theoretical results, the polar oxide surfaces can be stabilized via charge transfer between the upper and lower surfaces [25,26], adsorption of external atoms [25–27], and stoichiometry variations [29]. For  $\text{Zn}_{1-x}\text{Mg}_x\text{O}/\text{ZnO}$  heterostructures, we consider the effects of adsorption (hydrogen atoms, OH groups, and oxygen atoms) and stoichiometry variations (defects) on the electronic structures of  $\text{Zn}_{1-x}\text{Mg}_x\text{O}/\text{ZnO}$  ( $x = 0.25$  and  $0.50$ ) heterostructures. Through structural relaxations, it is found that the hydrogen atoms prefer to be adsorbed atop the zinc atom (on-top site), while the preferred adsorption sites for the OH groups and oxygen atoms are the fcc-hollow sites [see Fig. 1(b)]. Our results are consistent with those in Refs. [25–27]. For the  $2 \times 2$  in-plane (001)  $\text{Zn}_{1-x}\text{Mg}_x\text{O}$

supercell, the numbers of the on-top and fcc-hollow sites are both 4. In our calculations, the coverages of hydrogen atoms, OH groups, and oxygen atoms adsorbed on the surface of  $\text{Zn}_{1-x}\text{Mg}_x\text{O}$  are 50%, 50%, and 25%, respectively, while the concentration of vacancies on the Zn or Mg sites is 25% [25–27]. Specifically, for the  $x = 0.25$  heterostructure, the absorption sites of the hydrogen atoms are set on the top of the zinc atoms at positions 1 and 4 [see Fig. 1(b)]; the adsorption sites for the OH groups are set at fcc-hollow positions located at the top of the arrow and the position of the black dot; the fcc-hollow position at the top of the arrow is also set as the adsorption site of oxygen atoms; the Zn vacancies are obtained via removing the zinc atoms located at position 1.

Figure 5(b) shows the electrostatic potential of the  $\text{Zn}_{0.75}\text{Mg}_{0.25}\text{O}/\text{ZnO}$  heterostructure with hydrogen atoms adsorbed on the  $\text{Zn}_{0.75}\text{Mg}_{0.25}\text{O}$  surface (and with 42 Zn-O and 18 Zn-Mg-O layers). The results for the  $\text{Zn}_{0.75}\text{Mg}_{0.25}\text{O}$  surface with oxygen atom adsorption, OH group adsorption, and Zn or Mg vacancies are similar to that shown in Fig. 5(b). The macroscopic average potential on the ZnO side remains nearly a constant after the adsorption of hydrogen atoms. On the  $\text{Zn}_{0.75}\text{Mg}_{0.25}\text{O}$  side, the macroscopic average potential is almost insensitive to the position from L1 to L9 layers, and then slightly increases with increasing distance to the interface. An electrostatic field (with a magnitude of  $\sim 0.038 \text{ V}/\text{\AA}$ ) along the positive direction of the horizontal axis of Fig. 5(b) exists between the L10 and L18 layers. Thus surface adsorption or metal ion vacancies could really stabilize the polar surfaces of the  $\text{Zn}_{1-x}\text{Mg}_x\text{O}/\text{ZnO}$  ( $x = 0.25$  and  $0.50$ ) heterostructures.

The electronic structures of the  $\text{Zn}_{1-x}\text{Mg}_x\text{O}/\text{ZnO}$  ( $x = 0.25$  and  $0.50$ ) heterostructures with exotic-atom-adsorbed surfaces or with surfaces having metal ion vacancies, have been also calculated. Employing the modified GGA+ $U$  method, one can see that the electronic structures of the heterostructures reveal semiconductor characteristics when the surface contains metal ion vacancies, while the electronic structures exhibit metallic characteristics as the hydrogen, oxygen atoms, and OH groups are adsorbed on the surfaces, respectively. Next we mainly discuss the electronic structures of these heterostructures with hydrogen, oxygen atoms, and OH groups adsorbed on the surfaces calculated by the conventional GGA+ $U$  method. We use the electronic structures of the heterostructures with hydrogen-atom-adsorbed surfaces as examples to discuss the nature of these heterojunctions. Figure 6(a) shows the band structure (near the Fermi level) along some high-symmetry lines in the Brillouin zone for the hydrogen-adsorbed  $\text{Zn}_{0.75}\text{Mg}_{0.25}\text{O}/\text{ZnO}$  heterostructure (42 Zn-O and 18 Zn-Mg-O layers). Clearly, the Fermi level is located in the conduction band, and at the same time the absorption of the two hydrogen atoms in the  $2 \times 2$  in-plane supercell introduces two defect bands near the bottom of the conduction band. For this configuration (a hydrogen-adsorbed  $\text{Zn}_{0.75}\text{Mg}_{0.25}\text{O}/\text{ZnO}$  heterostructure with 42 Zn-O and 18 Zn-Mg-O layers), an oxygen vacancy at the most easily formed position (L1 layer) would introduce an additional defect band below the defect bands of hydrogen atoms while other characters of the energy band in Fig. 6(a) are retained, as shown in Fig. 6(b). Thus, the absorption of hydrogen atoms on the

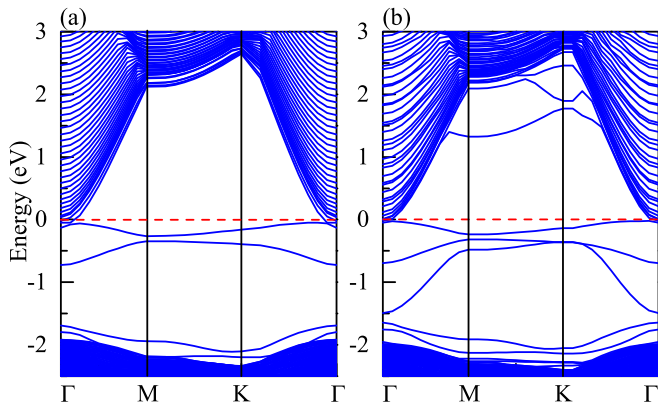


FIG. 6. The band structure for the  $\text{Zn}_{0.75}\text{Mg}_{0.25}\text{O}/\text{ZnO}$  heterostructures with surfaces of (a) hydrogen-atom absorption, and (b) hydrogen-atom absorption and with oxygen vacancies in  $\text{L}\bar{1}$ .

surface of the  $\text{Zn}_{0.75}\text{Mg}_{0.25}\text{O}/\text{ZnO}$  heterostructures will make the devices possess a metal-like band structure.

To obtain detailed information of the electronic structure, we calculated the partial DOS of each atomic layer for  $\text{Zn}_{1-x}\text{Mg}_x\text{O}/\text{ZnO}$  ( $x = 0.25$  and  $0.50$ ) heterostructures with exotic-atom-adsorbed surfaces. Figure 7(a) shows the partial DOS decomposed to the atomic layers for hydrogen-adsorbed  $\text{Zn}_{0.75}\text{Mg}_{0.25}\text{O}/\text{ZnO}$  heterostructures (42 Zn-O and 18 Zn-Mg-O layers). Clearly, the adsorption of hydrogen atoms on

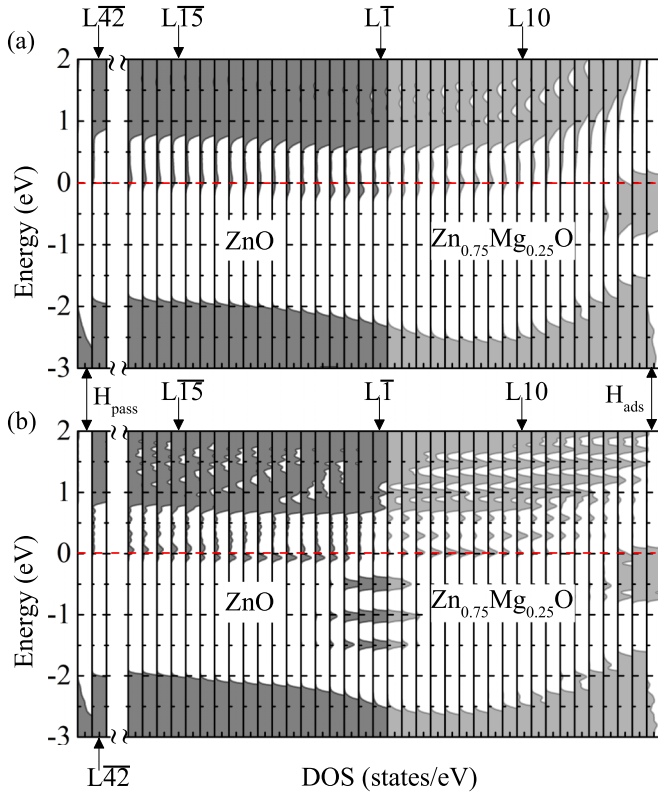


FIG. 7. The partial DOS projected onto the atomic layers for the  $\text{Zn}_{0.75}\text{Mg}_{0.25}\text{O}/\text{ZnO}$  heterostructures with surfaces of (a) hydrogen-atom absorption, and (b) hydrogen-atom absorption and with oxygen vacancies in  $\text{L}\bar{1}$ .

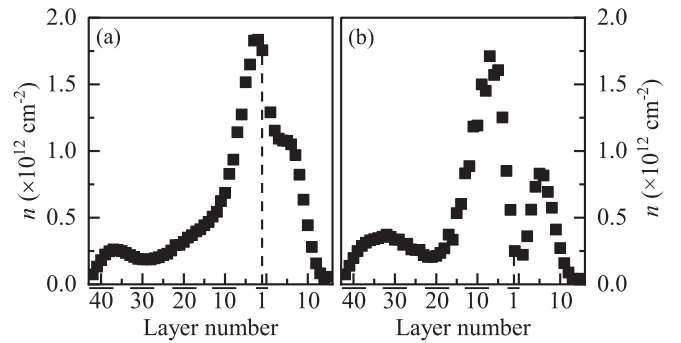


FIG. 8. The carrier concentration of each atomic layer for the  $\text{Zn}_{0.75}\text{Mg}_{0.25}\text{O}/\text{ZnO}$  heterostructures with surfaces of (a) hydrogen-atom absorption, and (b) hydrogen-atom absorption and with oxygen vacancies in  $\text{L}\bar{1}$ .

the surface introduces defect states near the Fermi level (partially higher than the Fermi level). As a result, the defect bands overlap with the conduction band, which renders the heterostructure to exhibit metallic characteristics in electronic structures. Although the polarization field distributed in the L10 to L18 Zn-Mg-O layers has significantly lifted up the top of the valence band, the valence band is still far from overlapping with the conduction band. In Fig. 7(b), we give the partial DOS projected onto the atomic layers for the hydrogen-adsorbed  $\text{Zn}_{0.75}\text{Mg}_{0.25}\text{O}/\text{ZnO}$  heterostructure (with 42 Zn-O and 18 Zn-Mg-O layers) with oxygen vacancies in  $\text{L}\bar{1}$ . Comparing to the partial DOS of the heterostructure without oxygen vacancies [Fig. 7(a)], one can see that oxygen vacancies in  $\text{L}\bar{1}$  introduce an extra defect band below the bottom of the conduction band. Although the defect band has no contribution to the conduction electrons in the conduction band, it changes the DOS around the Fermi level in the vicinity of the interface of the heterostructure (see further remarks below). For the oxygen-atom- or OH-group-adsorption case, the electronic structures are similar to those shown in Figs. 6 and 7.

Integrating the partial DOS from the bottom of the conduction band to the Fermi level, one can readily obtain the electron concentration of each atomic layer. Figures 8(a) and 8(b) show the electron concentration of each atomic layer for the hydrogen-adsorbed  $\text{Zn}_{0.75}\text{Mg}_{0.25}\text{O}/\text{ZnO}$  heterostructures (42 Zn-O and 18 Zn-Mg-O layers) without and with oxygen vacancies, respectively. For a heterostructure without oxygen vacancies, the electrons are mainly distributed from the  $\text{L}\bar{1}\bar{1}$  to L9 layers ( $\sim 5.0$  nm), while the electrons are mainly distributed from the  $\text{L}\bar{1}\bar{6}$  to L9 layers ( $\sim 6.3$  nm) for the heterostructure with oxygen vacancies in the  $\text{L}\bar{1}$  layer. Thus the heterostructures would reveal 2D or quasi-2D behaviors in the transport properties. Inspection of Fig. 8 indicates that the introduction of oxygen vacancies in  $\text{L}\bar{1}$  makes the electron concentration sharply decrease in the vicinity of the interface and the peak of the electron concentration shifts from the  $\text{L}\bar{2}$  layer to the  $\text{L}\bar{7}$  layer comparing with that for a heterostructure without oxygen vacancies. The carrier concentration maxima shown in Figs. 8(a) and 8(b) are both around  $1.8 \times 10^{12} \text{ cm}^{-2}$  ( $1.8 \times 10^{19} \text{ cm}^{-3}$ ), which is close to the experimental value [14,49]. In addition, the calculated

electron distribution range is also comparable to the experimental value [14,49].

The electronic structures of the heterostructures with an oxygen-atom-adsorbed or OH-group-adsorbed surface are similar to those for the hydrogen-adsorbed heterostructure. In addition, the introduction of oxygen vacancies in the Zn-O layer near the interface does not change the semiconductor characteristic of the electronic structure for the heterostructure with metal ion vacancies on the surface of the  $\text{Zn}_{1-x}\text{Mg}_x\text{O}$  film. Thus, for a  $\text{Zn}_{0.75}\text{Mg}_{0.25}\text{O}/\text{ZnO}$  heterostructure with a thin  $\text{Zn}_{1-x}\text{Mg}_x\text{O}$  film, the adsorption of hydrogen atoms, oxygen atoms, or OH groups on the surface of the  $\text{Zn}_{1-x}\text{Mg}_x\text{O}$  layer is responsible for the formation of 2DEG near the interface.

#### IV. CONCLUSIONS

In summary, to explore the origin of 2DEGs in  $\text{Zn}_{1-x}\text{Mg}_x\text{O}/\text{ZnO}$  heterostructures, we constructed  $\text{Zn}_{1-x}\text{Mg}_x\text{O}/\text{ZnO}$  ( $x = 0.25$  and  $0.50$ ) heterostructures

with different surfaces and investigated their electronic structures by first-principles calculations. It is found that the polarity discontinuity near the interface can neither lead to the formation of 2DEGs in devices with thick  $\text{Zn}_{1-x}\text{Mg}_x\text{O}$  layers nor in devices with thin  $\text{Zn}_{1-x}\text{Mg}_x\text{O}$  layers. For heterostructures with thick  $\text{Zn}_{1-x}\text{Mg}_x\text{O}$  layers, the oxygen vacancies near the interface are the source of the 2DEGs. For heterostructures with thin  $\text{Zn}_{1-x}\text{Mg}_x\text{O}$  layers, adsorption of hydrogen atoms, oxygen atoms, or OH groups on the surface of  $\text{Zn}_{1-x}\text{Mg}_x\text{O}$  films can not only stabilize the polar surface of  $\text{Zn}_{1-x}\text{Mg}_x\text{O}$  layer, but also cause the formation of 2DEGs near the interfaces of the devices.

#### ACKNOWLEDGMENTS

The calculation was conducted on the CJQS-HPC platform at Tianjin University. This work is supported by the National Natural Science Foundation of China through Grant No. 12174282.

- 
- [1] A. Ohtomo and H. Y. Hwang, A high-mobility electron gas at the  $\text{LaAlO}_3/\text{SrTiO}_3$  heterointerface, *Nature (London)* **427**, 423 (2004).
- [2] K. Koike, K. Hama, I. Nakashima, G. Takada, M. Ozaki, K. Ogata, S. Sasa, M. Inoue, and M. Yano, Piezoelectric carrier confinement by lattice mismatch at  $\text{ZnO}/\text{Zn}_{0.6}\text{Mg}_{0.4}\text{O}$  heterointerface, *Jpn. J. Appl. Phys.* **43**, L1372 (2004).
- [3] A. Tsukazaki, A. Ohtomo, T. Kita, Y. Ohno, H. Ohno, and M. Kawasaki, Quantum Hall effect in polar oxide heterostructures, *Science* **315**, 1388 (2007).
- [4] A. Tsukazaki, S. Akasaka, K. Nakahara, Y. Ohno, H. Ohno, D. Maryenko, A. Ohtomo, and M. Kawasaki, Observation of the fractional quantum Hall effect in an oxide, *Nat. Mater.* **9**, 889 (2010).
- [5] S. W. Lee, J. Heo, and R. G. Gordon, Origin of the self-limited electron densities at  $\text{Al}_2\text{O}_3/\text{SrTiO}_3$ , *Nanoscale* **5**, 8940 (2013).
- [6] P. Schütz, F. Pfaff, P. Scheiderer, Y. Z. Chen, N. Pryds, M. Gorgoi, M. Sing and R. Claessen, Band bending and alignment at the spinel/perovskite  $\gamma\text{-Al}_2\text{O}_3/\text{SrTiO}_3$  heterointerface, *Phys. Rev. B* **91**, 165118 (2015).
- [7] H. Zhang, Y. Yun, X. Zhang, H. Zhang, Y. Ma, X. Yan, F. Wang, G. Li, R. Li, T. Khan, Y. Chen, W. Liu, F. Hu, B. Liu, B. Shen, W. Han, and J. Sun, High-Mobility Spin-Polarized Two-Dimensional Electron Gases at  $\text{EuO}/\text{KTaO}_3$  Interfaces, *Phys. Rev. Lett.* **121**, 116803 (2018).
- [8] Y. Zhang, A. Neal, Z. Xia, C. Joishi, J. M. Johnson, Y. Zheng, S. Bajaj, M. Brenner, D. Dorsey, K. Chabak, G. Jessen, J. Hwang, S. Mou, J. P. Heremans, and S. Rajan, Demonstration of high mobility and quantum transport in modulation-doped  $\beta\text{-(Al}_x\text{Ga}_{1-x})_2\text{O}_3/\text{Ga}_2\text{O}_3$  heterostructures, *Appl. Phys. Lett.* **112**, 173502 (2018).
- [9] Z. Chen, Y. Liu, H. Zhang, Z. Liu, H. Tian, Y. Sun, M. Zhang, Y. Zhou, J. Sun, and Y. Xie, Electric field control of superconductivity at the  $\text{LaAlO}_3/\text{KTaO}_3$  (111) interface, *Science* **372**, 721 (2021).
- [10] J. Falson, Y. Kozuka, M. Uchida, J. H. Smet, T. Arima, A. Tsukazaki, and M. Kawasaki,  $\text{MgZnO}/\text{ZnO}$  heterostructures with electron mobility exceeding  $1 \times 10^6$   $\text{cm}^2/\text{V s}$ , *Sci. Rep.* **6**, 26598 (2016).
- [11] H. A. Chin, I. C. Cheng, C. I. Huang, Y. R. Wu, W. S. Lu, W. L. Lee, J. Z. Chen, K. C. Chiu, and T. S. Lin, Two dimensional electron gases in polycrystalline  $\text{MgZnO}/\text{ZnO}$  heterostructures grown by rf-sputtering process, *J. Appl. Phys.* **108**, 054503 (2010).
- [12] J. Ye, S. Ter Lim, M. Bosman, S. Gu, Y. Zheng, H. H. Tan, C. Jagadish, X. Sun, and K. L. Teo, Spin-polarized wide electron slabs in functionally graded polar oxide heterostructures, *Sci. Rep.* **2**, 533 (2012).
- [13] T. Makino, Y. Segawa, A. Tsukazaki, H. Saito, S. Takeyama, S. Akasaka, K. Nakahara, and M. Kawasaki, Magneto-photoluminescence of charged excitons from  $\text{Mg}_x\text{Zn}_{1-x}\text{O}/\text{ZnO}$  heterojunctions, *Phys. Rev. B* **87**, 085312 (2013).
- [14] H. Tampo, H. Shibata, K. Maejima, A. Yamada, K. Matsubara, P. Fons, S. Kashiwaya, S. Niki, Y. Chiba, T. Wakamatsu, and H. Kanie, Polarization-induced two-dimensional electron gases in  $\text{ZnMgO}/\text{ZnO}$  heterostructures, *Appl. Phys. Lett.* **93**, 202104 (2008).
- [15] H. Tampo, H. Shibata, K. Maejima, T. W. Chiu, H. Itoh, A. Yamada, K. Matsubara, P. Fons, Y. Chiba, T. Wakamatsu, Y. Takeshita, H. Kanie, and S. Niki, Band profiles of  $\text{ZnMgO}/\text{ZnO}$  heterostructures confirmed by Kelvin probe force microscopy, *Appl. Phys. Lett.* **94**, 242107 (2009).
- [16] J. D. Ye, S. Pannirselvam, S. T. Lim, J. F. Bi, X. W. Sun, G. Q. Lo, and K. L. Teo, Two-dimensional electron gas in Zn-polar  $\text{ZnMgO}/\text{ZnO}$  heterostructure grown by metal-organic vapor phase epitaxy, *Appl. Phys. Lett.* **97**, 111908 (2010).
- [17] J. Falson, D. Maryenko, Y. Kozuka, A. Tsukazaki, and M. Kawasaki, Magnesium doping controlled density and mobility of two-dimensional electron gas in  $\text{Mg}_x\text{Zn}_{1-x}\text{O}/\text{ZnO}$  heterostructures, *Appl. Phys. Express* **4**, 091101 (2011).
- [18] J. D. Hwang, C. C. Yang, and C. M. Chu,  $\text{MgZnO}/\text{ZnO}$  two-dimensional electron gas photodetectors fabricated by radio frequency sputtering, *ACS Appl. Mater. Interfaces* **9**, 23904 (2017).

- [19] K. Imasaka, J. Falson, Y. Kozuka, A. Tsukazaki, and M. Kawasaki, Spontaneous polarization driven MgZnO/ZnO heterostructures, *Appl. Phys. Lett.* **104**, 242112 (2014).
- [20] S. Akasaka, A. Tsukazaki, K. Nakahara, A. Ohtomo, and M. Kawasaki, Improvement of electron mobility above 100 000  $\text{cm}^2 \text{V}^{-1} \text{s}^{-1}$  in  $\text{Mg}_x\text{Zn}_{1-x}\text{O}/\text{ZnO}$  heterostructures, *Jpn. J. Appl. Phys.* **50**, 080215 (2011).
- [21] S. H. Yoo, M. Todorova, D. Wickramaratne, L. Weston, C. G. V. de Walle, and J. Neugebauer, Finite-size correction for slab supercell calculation of materials with spontaneous polarization, *npj Comput. Mater.* **7**, 58 (2021).
- [22] K. A. Brown, S. He, D. J. Eichelsdoerfer, M. Huang, I. Levy, H. Lee, S. Ryu, P. Irvin, J. Mendez-Arroyo, C. A. Mirkin, and J. Levy, Giant conductivity switching of  $\text{LaAlO}_3/\text{SrTiO}_3$  heterointerfaces governed by surface protonation, *Nat. Commun.* **5**, 5019 (2014).
- [23] X. Huang, E. Lindgren, and J. R. Chelikowsky, Surface passivation method for semiconductor nanostructures, *Phys. Rev. B* **71**, 165328 (2005).
- [24] H. Tampo, H. Shibata, K. Maejima, A. Yamada, K. Matsubara, P. Fons, S. Niki, T. Tainaka, Y. Chiba, and H. Kanie, Strong excitonic transition of  $\text{Zn}_{1-x}\text{Mg}_x\text{O}$  alloy, *Appl. Phys. Lett.* **91**, 261907 (2007).
- [25] G. Kresse, O. Dulub, and U. Diebold, Competing stabilization mechanism for the polar ZnO(0001)-Zn, *Phys. Rev. B* **68**, 245409 (2003).
- [26] O. Dulub, U. Diebold and G. Kresse, Novel Stabilization Mechanism on Polar Surfaces: ZnO(0001)-Zn, *Phys. Rev. Lett.* **90**, 016102 (2003).
- [27] M. Valtiner, M. Todorova, G. Grundmeier, and J. Neugebauer, Temperature Stabilized Surface Reconstructions at Polar ZnO(0001), *Phys. Rev. Lett.* **103**, 065502 (2009).
- [28] For a ZnO ( $\text{Zn}_{1-x}\text{Mg}_x\text{O}$  with  $x = 0.25$  or  $0.50$ ) slab with 18 Zn-O (Zn-Mg-O) layers, it is found that the polarization field inside the slab is nullified after the oxygen-terminated surface is passivated by pseudo-H atoms with  $0.48e$  and the Zn- (Zn-Mg-) terminated surface is passivated by pseudo-H atoms with  $1.52e$ . At the same time, the electronic structure of the passivated slab is similar to that of the bulk ZnO ( $\text{Zn}_{1-x}\text{Mg}_x\text{O}$ ).
- [29] J. Goniakowski, F. Finocchi, and C. Noguera, Polarity of oxide surfaces and nanostructures, *Rep. Prog. Phys.* **71**, 016501 (2008).
- [30] J. V. Lauritsen, S. Porsgaard, M. K. Rasmussen, M. C. R. Jensen, R. Bechstein, K. Meinander, B. S. Clausen, S. Helveg, R. Wahl, G. Kresse, and F. Besenbacher, Stabilization principles for polar surfaces of ZnO, *ACS Nano* **5**, 5987 (2011).
- [31] B. Meyer, First-principles study of the polar O-terminated ZnO surface in thermodynamic equilibrium with oxygen and hydrogen, *Phys. Rev. B* **69**, 045416 (2004).
- [32] A. Calzolari, M. Bazzani, and A. Catellani, Dipolar and charge transfer effects on the atomic stabilization of ZnO polar surfaces, *Surf. Sci.* **607**, 181 (2013).
- [33] O. Bengone, M. Alouani, P. Blöchl, and J. Hugel, Implementation of the projector augmented-wave LDA+ $U$  method: Application to the electronic structure of NiO, *Phys. Rev. B* **62**, 16392 (2000).
- [34] A. Rohrbach, J. Hafner, and G. Kresse, Electronic correlation effects in transition-metal sulfides, *J. Phys.: Condens. Matter* **15**, 979 (2003).
- [35] F. Oba, A. Togo, I. Tanaka, J. Paier, and G. Kresse, Defect energetics in ZnO: A hybrid Hartree-Fock density functional study, *Phys. Rev. B* **77**, 245202 (2008).
- [36] J. Paier, M. Marsman, and G. Kresse, Why does the B3LYP hybrid functional fail for metals? *J. Chem. Phys.* **127**, 024103 (2007).
- [37] Z.-H. Yang, H. Peng, J. Sun, and J. P. Perdew, More realistic band gaps from meta-generalized gradient approximations: Only in a generalized Kohn-Sham scheme, *Phys. Rev. B* **93**, 205205 (2016).
- [38] M. Shishkin, and G. Kresse, Implementation and performance of the frequency-dependent  $GW$  method within the PAW framework, *Phys. Rev. B* **74**, 035101 (2006).
- [39] T. R. Paudel and W. R. L. Lambrecht, First-principles calculation of the O vacancy in ZnO: A self-consistent gap-corrected approach, *Phys. Rev. B* **77**, 205202 (2008).
- [40] Ü. Özgür, Ya. I. Alivov, C. Liu, A. Teke, M. A. Reshchikov, S. Doğan, V. Avrutin, S.-J. Cho, and H. Morkoc, A comprehensive review of ZnO materials and devices, *J. Appl. Phys.* **98**, 041301 (2005).
- [41] Y. Yang, J. H. Zhang, S. B. Hu, Y. B. Wu, J. C. Zhang, W. Ren and S. X. Cao, First-principles study of Ga-vacancy induced magnetism in  $\beta\text{-Ga}_2\text{O}_3$ , *Phys. Chem. Chem. Phys.* **19**, 28928 (2017).
- [42] H. X. Wang, Y. Yan, K. Li, X. B. Du, Z. H. Lan and H. M. Jin, Role of intrinsic defects in ferromagnetism of  $\text{SnO}_2$ : First-principles calculations, *Physica Status Solidi B* **247**, 444 (2010).
- [43] J. Lee and A. A. Demkov, Charge origin and localization at the  $n$ -type  $\text{SrTiO}_3/\text{LaAlO}_3$  interface, *Phys. Rev. B* **78**, 193104 (2008).
- [44] L. Liu, Z. Mei, A. Tang, A. Azarov, A. Kuznetsov, Q. K. Xue, and X. Du, Oxygen vacancies: The origin of  $n$ -type conductivity in ZnO, *Phys. Rev. B* **93**, 235305 (2016).
- [45] S. J. Clark, J. Robertson, S. Lany, and A. Zunger, Intrinsic defects in ZnO calculated by screened exchange and hybrid density functionals, *Phys. Rev. B* **81**, 115311 (2010).
- [46] A. Alkauskas and A. Pasquarello, Band-edge problem in the theoretical determination of defect energy levels: The O vacancy in ZnO as a benchmark case, *Phys. Rev. B* **84**, 125206 (2011).
- [47] Y. Li, S. N. Phattalung, S. Limpijumngong, J. Kim, and J. Yu, Formation of oxygen vacancies and charge carriers induced in the  $n$ -type interface of a  $\text{LaAlO}_3$  overlayer on  $\text{SrTiO}_3(001)$ , *Phys. Rev. B* **84**, 245307 (2011).
- [48] P. W. Tasker, The stability of ionic crystal surfaces, *J. Phys. C* **12**, 4977 (1979).
- [49] H. Tampo, H. Shibata, K. Matsubara, A. Yamada, P. Fons, and S. Niki, Two-dimensional electron gas in Zn polar  $\text{ZnMgO}/\text{ZnO}$  heterostructures grown by radical source molecular beam epitaxy, *Appl. Phys. Lett.* **89**, 132113 (2006).